ORIGINAL ARTICLE

Impact of chemical clogging on de-watering well productivity: numerical assessment

F. Larroque · M. Franceschi

Abstract Among the processes leading to a decrease in productivity, chemical clogging is often mentioned as one of the major features. De-watering of a confined aquifer caused by an unsuitable pumping scheme produces a phenomenon involving the diffusion of oxygen in the aquifer which disturbs the geochemical conditions in the initial system. Coupled chemical and transport processes are proposed in an assessment of the impact of de-watering on the precipitation of carbonate and iron oxide. The reactions are studied for waters showing low dissolved iron concentrations such as commonly observed in drinking water supplies. The quantity and distribution of precipitated iron oxide and calcium carbonate are used in a permeability model to calculate the productivity loss. For the conditions used in the simulations, the carbonate precipitate can be neglected compared to iron deposits which remain weak. The spatial distribution is heterogeneous and quite similar to the patterns observed in the field. This shape is mainly caused by a competition between the diffusion of oxygen due to the de-watering process and the rate of precipitation of iron oxide. However, the loss of well productivity remains moderate. It is clearly shown that de-watering of the well and the associated chemical incrustations that this induces cannot alone explain field data. More complex processes involving biological clogging and accurate hydrodynamic behaviour in the closest part of the well remain to be included in the modelling approach in order to provide valuable insights into the problem of well ageing.

Introduction

Well productivity during water extraction from unconfined and confined aquifers often decreases over time due to several interdependent physical, biological and chemical phenomena. Physical deterioration occurs when the well casing is damaged, corroded or when the permeability of the material surrounding the well decreases due to particle clogging. The theoretical and experimental study of such effects are treated as a hydrodynamic problem introducing the skin effect into pumping well equations, in a similar way to the petroleum industry (Barrash et al. 2006; Durlofsky 2000; Han and Dusseault 2003). Biological clogging can occur through several processes leading directly or indirectly to changes in hydraulic properties. Many researchers have documented the effect of on microorganisms on clogging and a list of references can be found in Wu et al. (2008). In more detail, two cases can be distinguished. Firstly, bio-fouling can occur through the accumulation of biological slime in the porous media in close vicinity to the well. The second mechanism corresponds to the catalytic role of micro organisms in some mineral precipitate processes (Houben and Treskatis 2007).

Currently, the most commonly cited reasons for explaining productivity variations involve a reduction of aquifer permeability due to chemical scaling in the well screen and deposition of materials around the intake portion of the well. Indeed, a study investigating 12,000 wells, performed in 1998 by the DVGW (German Technical and Scientific Association on Gas and Water), leads to the following statistics concerning well ageing processes (Houben 2003a):

F. Larroque (✉) · M. Franceschi
EA GHYMAC n°4134 EGID, Université de Bordeaux,
1 allee Daguin, 33607 Pessac, France
e-mail: larroque@egid.u-bordeaux3.fr

- Chemical processes account for 91% of the ageing in wells (mineral precipitation and corrosion);
- Physical processes leading to a decrease of productivity (sand intake for example) occur in 9% of the wells;
- Microbial slimes and biological clogging are of minor importance.

The formation of incrustations seriously affects the performance of wells or piezometers. Oxides of iron, manganese (ochre) and carbonates are the most usual precipitated mineral phases leading to partial or complete blocking of pore spaces in filter gravel and/or screen slots (Houben and Treskatis 2007). This phenomenon has been investigated for water wells and piezometers (Walter 1997; Hitchon 2000; Houben 2003a, b).

It appears that wells subjected to de-watering processes are more exposed to ageing issues and especially to the incrustation phenomena (Driscoll 1986). De-watering occurs in confined or semi-confined aquifers when the pumping-induced piezometric head falls below the overlying semi-permeable layer, leading to a local and limited unconfined aquifer around the pumping well (Fig. 1). Such situations can generally be avoided by an adequate exploitation scheme, but repeated de-watering phases very often lead to productivity losses. Indeed, the de-watering process is not in itself damaging for pumping installations but it does induce important modifications to the physical and the chemical equilibrium of the water within the aquifer around the well which leads to deposition of scale materials. The impact of scale deposits has been mentioned for long-term de-watering structures used, e.g., in excavation areas (Powers et al. 2007). The impact of de-watering and how it leads to chemical deposits has been described for pipes and horizontal drains installed in cut slopes (Leung et al. 2005), but no real quantitative approach seems to have been developed to clarify these processes in a complex environment. Moreover, to our knowledge, no data seem to exist for pumping wells in particular, despite the technical and economical importance of these

applications. The prevention of well ageing, particularly, and the improvement of rehabilitation techniques relate directly to this issue.

This paper describes a first framework for estimating the impact of de-watering processes on a pumping well within a simplified 3D numerical model. The aim of this modelling approach is to understand the application of the main physico-chemical processes involving chemical scaling, as much as their relative importance, using a simplified theoretical aquifer. Biological effects can now be integrated into permeability models (Freedman et al. 2005; Soleimani et al. 2009; Thullner et al. 2004) to describe the theoretical reduction in hydraulic properties caused by biomass growth, but applications in real-life situations are still limited.

So a 3D reaction/transport model was built and the implementation of the hydrochemical mechanisms induced by the de-watering process is presented here. The impact of these basic processes was studied and a sensitivity analysis of the model was performed to allow the identification of essential parameters requiring accurate description and quantification for future development. The objectives of the modelling approach presented here are essentially to plan further modelling tools integrating higher complexity in order to consider real-life applications.

Modelling frameworks

Groundwater flow model and numerical method

The test problem is designed to represent a simple confined groundwater system with significant withdrawals at one pumping well. Drastic drawdown at the well leads to a local and partial de-watering of the confining aquifer. This hypothetical study is based on the general characteristics of a local aquifer and a representative compilation of well exploitation conditions in the South West of France, near the city of Bordeaux.

The computer model used in this study to simulate 3D transport around the pumping well is a finite-difference code developed by the USGS called PHAST (Parkhurst et al. 2004). PHAST is a combination of the geochemical code PHREEQC (Parkhurst and Appelo 1999) and the finite-difference flow and transport code HST3D (Kipp 1987). It is a general purpose code that can accurately simulate flow, transport and chemical processes controlled by chemical equilibrium or reaction kinetics. Input data for the flow and transport simulations were constructed using GOPHAST (Winston 2006), a graphical user interface for interacting with the PHAST code. Post-processing data analysis was performed using several programs including Model Viewer (Hsieh and Winston 2002) and MATLAB^{TM}.
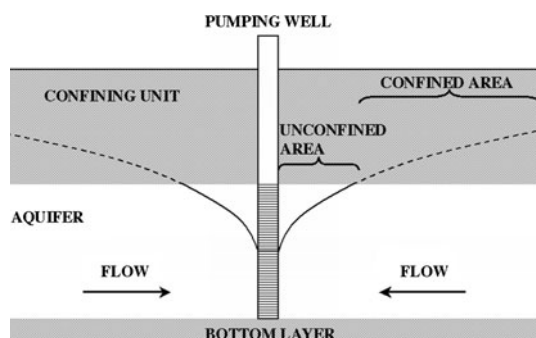

Fig. 1 Conceptualisation of de-watering problem for a pumping well in a confined aquifer leading to the formation of unsaturated area in the closest part of the well
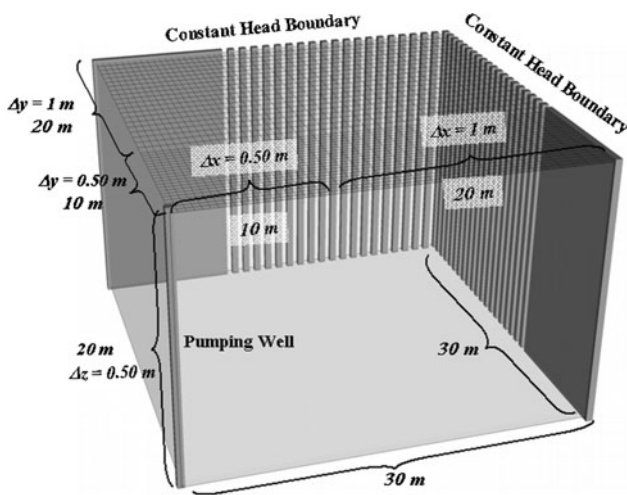
Fig. 2 PHAST 3D discretization scheme used for the numerical de-watering simulation based on telescopic mesh

The model is designed to represent a confined aquifer system in which significant groundwater withdrawals from a unique well occur. The domain is considered homogeneous. To increase the efficiency of the flow and transport simulations, hydrological symmetry rules were applied in the conceptualisation of the model and discretization of space. Only a quarter section of the well and aquifer domain is taken into account, thanks to the radial symmetry of the system (Fig. 2). The hypothetical 20 m thick aquifer is divided into 40 layers each 0.5 m thick. In the x and y directions, a telescopic mesh is used. It includes a first mesh of 0.5 m node spacing starting from the well and reaching outwards to 10 m. Then a second, larger mesh of 1 m node spacing extending 20 m in both lateral directions is applied. The discretization scheme yields a total of 64,000 active cells.

The choice of symmetry rules (a quarter part of the flow field) is made based on the consideration that only the flow field generated by the pumping well is of interest here. So the flow field can be considered locally as radially convergent. According to this approach, the natural ground water regime is neglected.

The aquifer of the domain is initially confined and is considered to be homogeneous and isotropic. The hydraulic conductivity K of the background aquifer materials is assumed to be constant and the value is 5×10^{-5} m s^{-1}. The porosity of the material is set arbitrarily to 0.25. Spatial dimensions of the aquifer are not of interest here due to the local area of study.

The geometrical and hydrodynamic parameters applied in this approach correspond to mean values observed in the first shallow confined aquifers in the South West of France used for drinking water supplies (Andre 2002; Douez 2007; Larroque 2004, Larroque et al. 2008). However, these

values remain theoretical values for other hydrological systems. They are used here as representative synthetic parameters for the modelling approach and therefore cannot be considered as exhaustive for all groundwater systems used for drinking water exploitation.

Well conditions corresponding to the Neumann boundary limits are set in the South East corner over the total thickness of the aquifer (Fig. 2). Opposite sides of the well are represented as constant head boundaries (Dirichlet condition). Due to symmetry rules, the same constant head is retained on both sides. For this hypothetical study, the boundary value for constant head can be set to an arbitrary number, representative of a confined condition. The pumping rate must be sized to produce local de-watering of the aquifer under particular initial hydrodynamic conditions. To proceed to this sizing, Thiem's analytical formulation for steady flow into a well in a confined aquifer was used (Bear 1979):

$$s = \frac{Q_w}{2\pi T} \ln \frac{R}{r_w} \qquad (1)$$

where s is the drawdown at the well, Q_w is the pumping rate of the well, T is the transmissivity of the aquifer, r_w is the distance from the well axis where drawdown is considered and R is the radius of influence of the well, i.e. the distance beyond which drawdown is negligible or unobservable. R corresponds in the numerical model to the distance of the well from the constant head boundaries (30 m). The value of the constant head was set arbitrarily at 32 m. A value for the pumping rate q_0 of 75 m^3 h^{-1} was applied for the well. The value in the numerical model corresponds to a quarter of the value applied in the analytical solution, i.e. 18.75 m^3 h^{-1}. The results obtained by both solutions (numerical and analytical) for the set of applied parameters emphasize the consistency of the discretization scheme for numerical simulation of steady-state groundwater flow (Fig. 3).
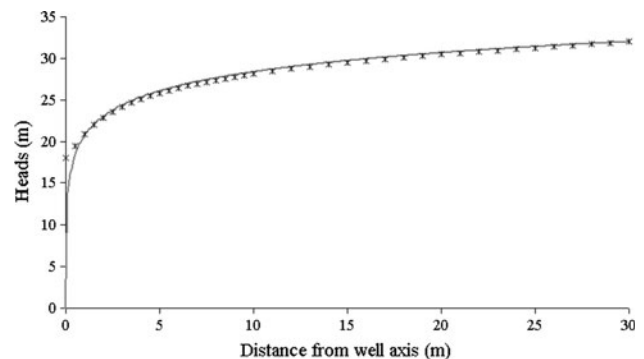

Fig. 3 Heads computed for the steady-state pumping configuration using Thiem's analytical solution (*grey line*) and the numerical PHAST model (*black crosses*)
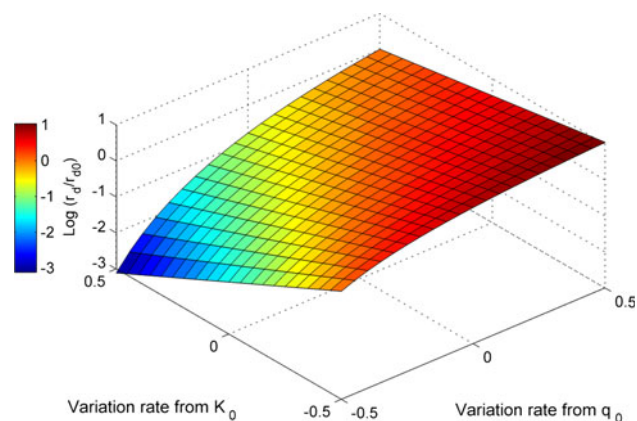
Fig. 4 Standardized de-watering radius (r_d/r_{d0}) values for variations of the standard parameters K_0 and q_0 describing the basic hypothetical case

Equation 1 can be used to estimate the radius of de-watering r_{d0} for the basic hypothetical case. Introducing the value s_{max} corresponding to the maximum drawdown allowed before de-watering the aquifer, r_{d0} can be expressed as follows:

$$r_{d0} = \frac{R}{\exp\left(\frac{2\pi K_0 b s_{max}}{q_0}\right)} \qquad (2)$$

with b, the thickness of the aquifer, K_0, the hydraulic conductivity for the hypothetical basic case and q_0, the pumping rate of the well for the basic case.

Based on the parameters defined above and the values retained for both the analytical and the numerical model, the basic de-watering radius r_{d0} is 0.83 m. This radius corresponds to the maximum radius projected onto the ground surface. This value decreases quickly with depth since the drawdown surface is shaped like a cone. A sensitivity analysis was performed using Eq. 2 for the main parameters which affect the de-watering radius for given boundary limits, i.e. the pumping rate, q, and the hydraulic conductivity, K. The de-watering radius r_d was computed in this way for over a range of variation of 50% for both parameters q_0 and K_0 and normalized to the basic de-watering radius r_{d0} (Fig. 4). As expected from the Thiem formula and emphasized by Fig. 4, the standardized de-watering radius represented by this ratio emphasizes its sensitivity to hydraulic conductivity and pumping rate variations. In this representation, the hydraulic conductivity is assumed to be homogeneous. Only general variations are taken into account here, rather than the heterogeneous distribution inside the porous material. Given a constant value of conductivity, it appears that the choice of pumping rate is the determining factor for the size of the de-watered radius. As an example, a reduction of the standard pumping rate by 50% leads to a decrease by a factor close to 15

times in the size of the standard de-watered radius. This fact is a key element for the management of de-watering problems in pumping wells.

Hydrochemical transport basics and numerical implementation

Transport parameters are assumed to be homogeneous over the whole model. From symmetry, longitudinal and lateral dispersivities are assumed equal and only vertical anisotropy is included in the dispersivity. A ratio of 1/10 between vertical transverse and horizontal dispersivities is selected as it is generally accepted that vertical transverse dispersivity is typically about one order of magnitude smaller than the horizontal dispersivity (Gelhar et al. 1992). The mean value of dispersivity is a key element for chemical and transport simulations. The characterization of this parameter remains one of the major difficulties. Moreover, it is a known fact that this value is linked directly to the scale of observation (Gelhar et al. 1992; Boggs et al. 1992). So, we retained a plausible range of values for the horizontal dispersivity corresponding to the size of our modelling domain and to the potential scale of the area affected by scaling processes. A mean value of 2 m for the horizontal dispersivity was taken as a reference for the base case model. The vertical dispersivity corresponding to this value for the base case is 0.2 m. The sensitivity of this parameter is tested further in this paper.

Although the model can simulate dispersion, this phenomenon is only representative when the dispersion coefficient is greater than the inherent numerical dispersivity of the model. The numerical dispersivity is a function of the model cell size and of the computational time step used in the transient simulation of the reaction and transport processes. It can be approached approximately for a given flow direction by the relation (Sun 1996):

$$D_{num} = \frac{\Delta X}{2} + v\frac{\Delta t}{2} \qquad (3)$$

where D_{num} is the numerical dispersivity, ΔX is the cell dimension in the x direction, v is the flow velocity and Δt is the time step. So, Δt must be chosen to minimize the value of the numerical dispersion but small time steps lead to very high costs in terms of computational effort. A compromise solution was retained with a value for the time step of 30 min. This value does not completely prevent the numerical dispersion from affecting the model, but limits the computational time needed for transient simulations, even for long time durations, and it is consistent with the transport and chemical processes integrated in the model.

De-watering leads to exposure of the water column to atmospheric conditions including oxygen uptake and CO_2

degassing. In such conditions, the mixing of water containing oxygen with reduced groundwater leads to mineral incrustations, especially ferric iron. The formation of ferric iron incrustations can be described by the following equation:

$$4Fe^{2+} + O_2 + 10H_2O = 4Fe(OH)_{3(S)} + 8H^+ \qquad (4)$$
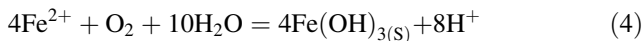
The kinetic rates are well documented in the literature (Singer and Stumm 1970; Sung and Morgan 1980; Millero 1985; Millero et al. 1987; Houben 2004) and can be expressed by:

$$r_{Fe} = k_{Fe_s} |Fe^{2+}| |O_2| |H^+|^{-2} \qquad (5)$$

The iron oxide formed has a catalytic effect and increases the reaction rate (Tamura et al. 1976; Houben 2004) and so a more complete rate law is:

$$r_{Fe} = k_{Fe1} |Fe^2| |O_2| |H^+|^{-2} + k_{Fe2} |Fe^3| |Fe^2| |O_2| |H^+|^{-2} \quad (6)$$

where k_{Fe1} is the constant rate for iron oxidation, k_{Fe2} is a global constant for adsorption of Fe^{2+} on ferric oxide and oxidation at the ferric oxide surface.

Calcium carbonate incrustations are associated with iron oxide precipitation due to degassing of carbon dioxide around the well when the flow regime becomes turbulent (Houben 2004). The equation can be expressed as:

$$Ca^{2+} + 2H_2CO_3^- = CaCO3_{3(S)} + CO_{2(g)} + H_2O \qquad (7)$$
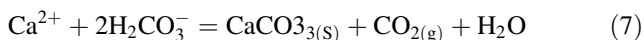
The classical PWP (Plummer-Wigley and Parkhurst) equation is used for the kinetic precipitation of $CaCO_3$ (Plummer et al. 1978):

$$r_C = k_1 |H^+| + k_2 |H_2CO_3| + k_3 |H_2O| - k_4 |HCO_3^-| \qquad (8)$$

where r_c is the general kinetic equation (precipitation and dissolution), $k1$, $k2$ and $k3$ are the rate constants for the forward reactions (dissolutions) and $k4$ is the rate constant for the backward reaction (precipitation).

The first three terms of Eq. 8 define the dissolution rate, r_d, and the last term defines the precipitation rate, r_p, and thus Eq. 8 remains applicable to both dissolution and precipitation. The precipitation rate depends on the composition of the solution. While a simplified water composition is used with a simplified CO_2–water–calcite system, the bicarbonate concentration is approximately equal to twice the calcium concentration and can be expressed as follows :

$$r_c = r_d \left[1 - \left(\frac{IAP_C}{K_{sC}} \right)^{2/3} \right] \qquad (9)$$

where r_d is the dissolution rate, IAP_C is the ionic activity product for $CaCO_3$, and K_{sC} is the solubility product for calcite at the solution temperature.

Application of model

The evolution of oxide precipitation induced by the dewatering process is considered for three kinds of interstitial water. The initial solution is typical of the groundwater composition used for drinking purposes. The same global composition with different amounts of Fe (Table 1) is retained. All the waters are near equilibrium with respect to calcite and with $PCO_2 = 10^{-2.5}$ atm. The first type is in equilibrium with Fe(OH)3 and FeCO3 and the others are supersaturated with respect to Fe(OH)3 and FeCO3. The aqueous compositions are simplified in comparison to real natural water; the influences of other ionic species (Na, K,...) are ignored.

Water 1 is representative of some waters found in the area of Bordeaux (Gironde, France) and presents a mean value of concentration for ferrous iron of 5.2×10^{-3} mmol/L (i.e. 0.28 mg/L). Water 2 is assumed to contain 10×10^{-3} mmol/L ferrous iron (i.e. 0.55 mg/L). Finally, water 3 presents a concentration of 20×10^{-3} mmol/L ferrous iron (i.e. 1.1 mg/L). This is based on the iron concentration in groundwater in the Oligocene aquifer in the South West of France outside the city of Bordeaux. This regional semi-confined/confined aquifer is mainly exploited as a supply of drinking water. A compilation of 1,522 analyses was exploited from 136 wells collected by the French Survey Agency for sanitary and health (Direction Départementale des Affaires Sanitaires et Sociales de la Gironde) between 1985 and 2007. The study of these data emphasizes that iron concentrations range from <3–4,700 μg/L. But for 95% of the analyses, iron concentrations are <20 mmol/L (1.12 mg/L). Groundwater samples with iron concentrations >20 mmol/L refer only to ten wells approximately, with particular mining conditions. The range of ferrous iron concentrations used for this work is low compared to classical values used for geochemical modelling of iron oxide incrustations (Houben 2004; Houben and Treskatis 2007) but remains more representative of deeper confined waters (André 2002) in the South West of France. The temperature of water ranges from 13 to 24°C in the same field data. An upper limit of 25°C was

Table 1 Hydrochemical facies of synthetic waters used for the numerical simulations

Variable	Water 1 (base case)	Water 2	Water 3
Temperature (°C)	25	25	25
pH	7.624	7.624	7.624
pe	0.528	0.528	0.528
C (mmol/L)	2.284	2.284	2.284
Ca (mmol/L)	1.089	1.089	1.089
Fe (10^{-3} mmol/L)	5.2	10	20

chosen for all simulations (Table 1). This maximum corresponds to enhanced precipitation of materials from the temperature-dependant chemical mechanism presented above.

Transient simulations are carried out for each hydrochemical composition for a total de-watering duration of 250 h.

In all the models, the simulations lead to solid deposits forming according to the chemical species introduced in the geochemical framework. The formation of ferric iron and carbonates is simulated. However, the quantity of carbonate obtained remains low for all kinds of water. The mass of carbonate is several orders of magnitude smaller than the ferrous oxides and shows the same general pattern as the oxide incrustations. It is true that the precipitation of carbonate is limited by the quantity of carbon dioxide. The modification of the groundwater equilibrium by the de-watering process produces only minor changes of CO_2 in the groundwater, limiting the development of carbonate scales. In pumping wells, the major part of CO_2 degassing should occur in the closest part of the well, induced by the higher water flow velocities which may be responsible for increased mixing (Houben 2004, 2006). The model developed here does not include accurate enough groundwater flow in the immediate vicinity of the well to reproduce the effects of CO_2 bubbling leading to the calculated quantity of carbonates deposit being underestimated.

So the study next focusses on the ferric iron incrustations which constitute the major share of the solid deposits and may cause a reduction in both porosity and permeability, by modification of the pore space geometry. It is important to bear in mind that carbonate deposits exist but remain low compared to iron scaling.

As expected from the chemical equations, an essential condition for understanding the spatial distribution of clogging is the mixing of ground waters with oxygen. So the pattern of ferric incrustations is directly linked to the dispersion of oxygen in the porous media from the de-watered region at the top of the aquifer. The vertical distribution of iron oxides precipitated after 250 h under de-watering conditions for water 1 (initial concentration in ferrous iron of 5.2×10^{-3} mmol/L) is presented in Fig. 5. The distribution presents a complex 3D structure, shown here as a 2D representation thanks to the symmetry applied in the groundwater model. Ferrous oxides are mainly precipitated in close proximity to the pumping well. On the well axis, incrustations tend to be more abundant in the upper part of the screened region than in the lower part. Indeed, the maximum value of weight is reached locally at between 2 and 3 m of depth. The upper part of the well remains only moderately affected. The rest of the screened well shows no incrustation processes.
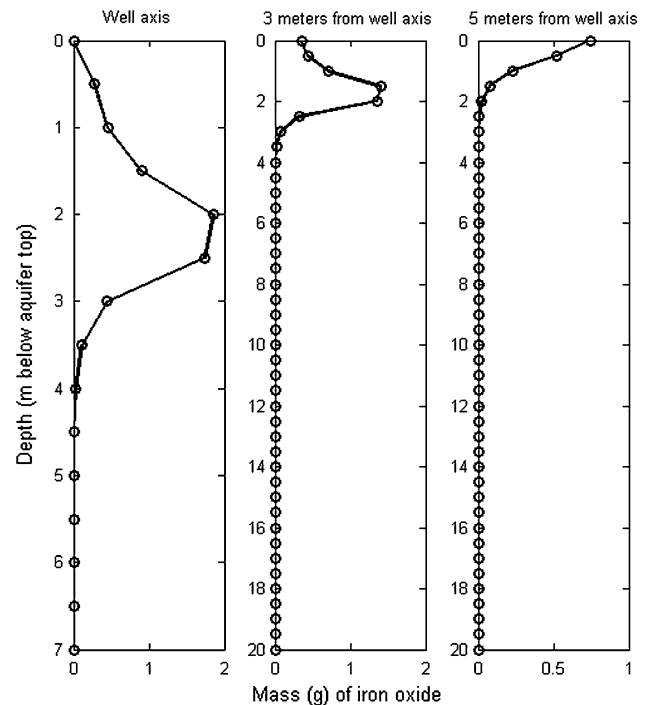

Fig. 5 Vertical distribution of iron oxide mass precipitated for the base case model at increasing distances from the well axis after 250 h of de-watering for water 1. The initial concentration of ferrous iron for water 1 is assumed to be 5.2×10^{-3} mmol/L

In the lateral direction away from the well axis, the shape of iron incrustations evolves with distance (Fig. 6). At 3 m from the well axis, although the general pattern of deposits remains comparable with that in the nearest part of the well, the amount of precipitated iron decreases. A noteworthy fact is the deposition of iron oxide at the top of the aquifer medium. The value computed after 250 h for water 1 is low (0.4 g) but increases with distance to reach a maximum (0.75 g) at around 5 m away from the well axis, before decreasing rapidly and returning to zero beyond that point. Thus, the spatial distribution in the vicinity of the well is clearly heterogeneous and seems to be represented by a curve-shaped structure. This structure corresponds to the region with significant oxygen dispersion from the de-watered area during over-exploitation of the well. The dimensions of the ellipsoidal curved shape are conditioned by the migration of dissolved oxygen in the aquifer. This phenomenon remains subject to the dispersivity properties of the porous medium and their relative ratio. A study of the sensitivity to these parameters and their impact on the simulated distribution of scaled mass is developed further.

From this first simulation, it is shown that the majority of incrustation occurs on the well axis and in the upper part of the screened region. The maximum level of deposit is reached more deeply here than at the top of the aquifer. On
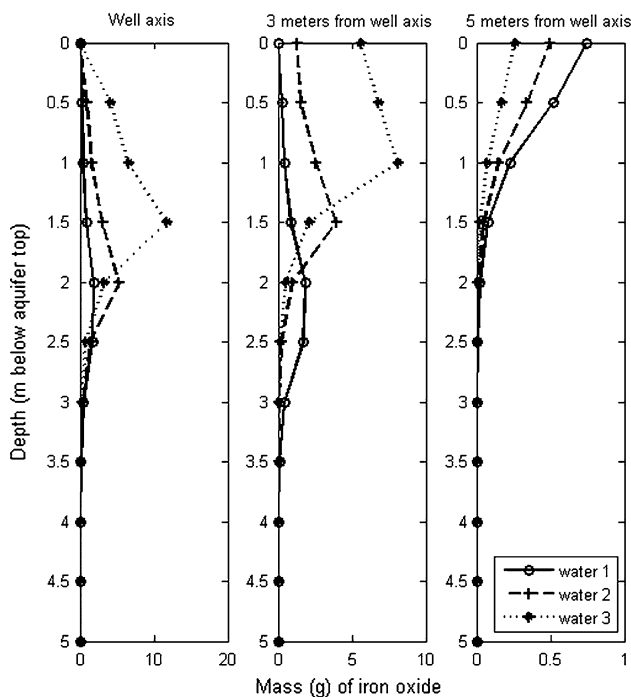
Fig. 6 Vertical distribution of iron oxide mass precipitated for increasing iron content in interstitial water for different distances from well axis (well axis, 3 m away from well axis and 5 m away from well axis). *Black circles* correspond to water 1 (ferrous iron = 5.2×10^{-3} mmol/L), *black crosses* correspond to water 2 (ferrous iron = 10×10^{-3} mmol/L) and *black stars* correspond to water 3 (ferrous iron = 20×10^{-3} mmol/L)

Fig. 7 Vertical distribution of relative weight of iron oxide precipitated after 250 h of de-watering condition for increasing contents of ferrous iron in interstitial water

the other hand, incrustations in the upper part of the aquifer can moderately affect the region of the well in close vicinity, at the point of contact between porous media and overlying aquitard.

The spatial distribution of iron oxides remains quite similar, considering the increasing amounts of ferrous iron in the interstitial water (Fig. 7). Indeed, the highly concentrated water (water 3) leads to a total mass of scaled iron of 13.44 g after 250 h under de-watering conditions. 80% of this mass is deposited at a depth between 1 and 2 m from the top of the aquifer, i.e. in the upper part of the screen. Going into more detail, a slight modification of the vertical distribution occurs between the lower (water 1) and higher (water 3) amounts of dissolved iron on the well axis. The maximum amount of iron deposits occur deeper for the less concentrated interstitial water. So the detailed shape of oxide deposits seems to be linked to the initial concentration of ferrous iron in the water.

As the chemical reactions of ferrous oxide incrustation are integrated into the model as kinetic phenomena, the impact of time must be detailed. As pointed out for the well axis in the case of water 1 (Fig. 8), the extra time under de-watering conditions, i.e. duration of mixing with oxygen, leads to a linear relationship for the amount of scaled
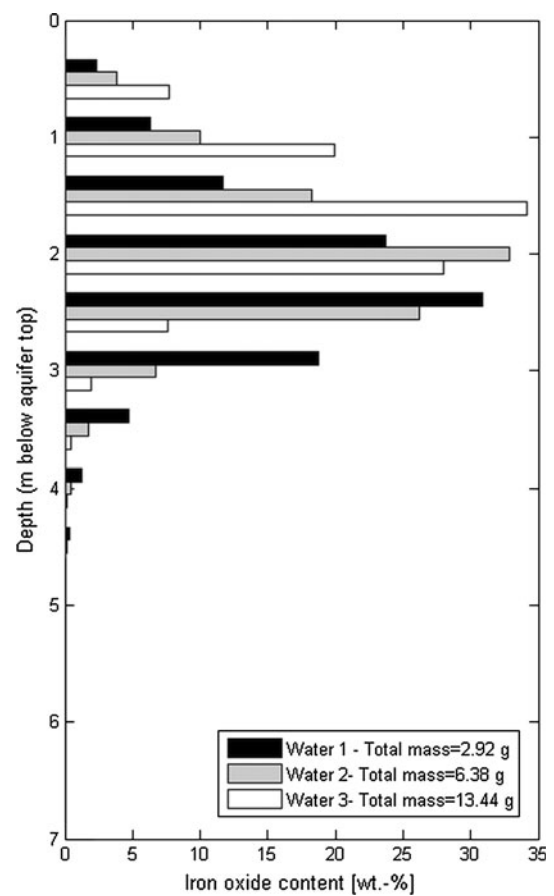
material. The pattern remains unchanged. The total quantities precipitated increase with respect to time. The study of a transient model for rising ferrous iron concentrations in interstitial waters (Fig. 9) reveals that the linearity is still maintained. Only the rate of iron precipitation is strongly linked to the initial concentration in the water, as expected from the linear kinetics of precipitation reactions. At this point, the constant rate of incrustation allows a quick projection of precipitated quantities for de-watering conditions of long duration without involving expensive computational work. An example of such a projection is carried out here for periods of 3,000, 15,000 and 30,000 h of de-watering (Table 2). Assuming a mean pumping time of 8 h per day, these simulations of different de-watering durations can be compared to a production time of approximately 1, 5 and 10 years. The maximum amount of precipitated oxide is reached on the well axis for water 3. 1,600 g of Fe(OH)3(S) materials are thus precipitated from the bottom of the upper aquitard through the aquifer. The thickness of the precipitation region remains <3 m on the well axis.
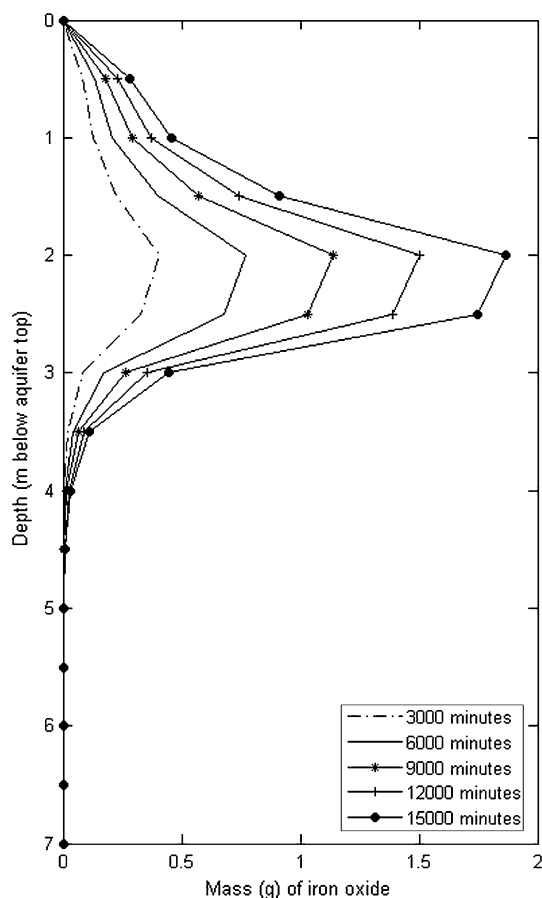
Fig. 8 Vertical distribution of iron oxide mass precipitated for the base case model for increasing time of de-watering conditions for water 1. The initial concentration of ferrous iron in water 1 is assumed to be 5.2×10^{-3} mmol/L
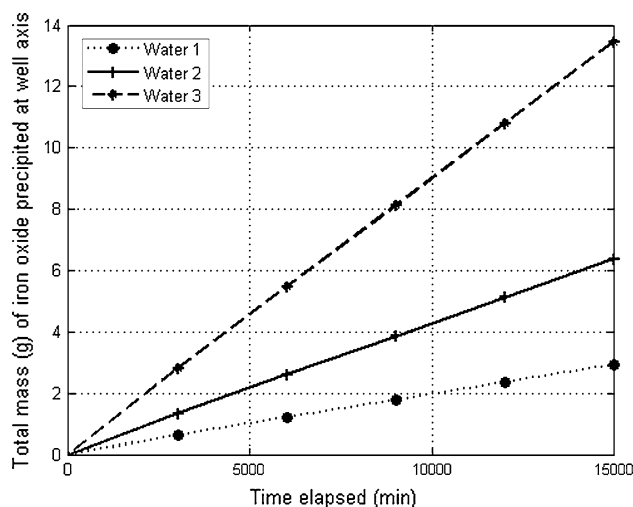

Fig. 9 Transient evolution of total mass of iron oxide precipitated at well axis for different initial composition of interstitial water. *Black dots* correspond to water 1 (ferrous iron = 5.2×10^{-3} mmol/L), *black crosses* correspond to water 2 (ferrous iron = 10×10^{-3} mmol/L) and *black stars* correspond to water 3 (ferrous iron = 20×10^{-3} mmol/L)

Discussion

The distribution of ferrous oxide induced by the introduction of oxygen into a confined aquifer system by means of local well de-watering is calculated. De-watering for a longer duration is employed. Three generic interstitial waters with increasing iron contents are considered. The results emphasize a complex pattern of iron deposition, with a maximum reached on the well axis, at a depth of around 2 m. The spreading of iron deposits in the lateral direction is clearly linked to the concentration of dissolved iron as emphasized by previous tests. In details, the shape and position of the iron incrustations are controlled by three transient processes.

- Groundwater flow and velocity of water particles (here assumed to be in steady state);
- Diffusion and transport of dissolved oxygen;
- Kinetic rate of iron oxide precipitation, linked to iron oxide concentration (Eq. 6).

As a result of these three combined processes, in the vicinity of the well, the rate of oxidation due to higher oxygen concentrations and the saturation with respect to iron oxides increase. At the same depth near the surface, the rate of iron oxidation and precipitation will be greater at the higher iron concentrations. Oxygen consumption is also more important, involving as it does a reduction in the rate of oxidation with depth, as the oxygen concentration decreases. At low iron concentration, the precipitation rate is lower and the oxygen concentration remains relatively important. Induced by the plentiful availability of oxygen, iron oxidation saturation is obtained.

The same process can explain differences between the lateral distances corresponding to maximum deposits. The higher concentration occurs farther from the well as the iron concentration decreases. As the oxygen consumption is less important for low iron concentration in close vicinity to the well, dispersion processes for the dissolved oxygen are more important and the peak in the reaction takes place farther away. Thus, the saturation with respect to iron oxide is obtained farther away from the well.

In the case presented here, iron oxide saturation is obtained at a shallower depth for water 3, and iron oxide precipitation occurs closest to the surface, e.g. closest to the well. For water characterized by lower iron concentrations (water 2 and water 1), saturation with respect to iron oxide occurs at greater depths and farther away, as is the case with precipitation.

To summarize, the shape of iron incrustations remains the same, but the position changes with iron concentration and rate of oxygen consumption.

Table 2 Weights (g) of iron oxide precipitated at the axis of the well during the life of the well, for a mean exploitation of 8 h per day, considering rising ferrous concentration in interstitial water

	Total iron oxide at well axis (g)			Total iron oxide at 3 m from well (g)			Total iron oxide at 5 m from well (g)		
	Water 1	Water 2	Water 3	Water 1	Water 2	Water 3	Water 1	Water 2	Water 3
1 year (3,000 h)	35.12	76.53	161.33	27.04	59.98	128.48	7.34	4.84	2.48
5 years (15,000 h)	175.62	382.65	806.63	135.21	299.93	615.92	36.73	24.21	12.40
10 years (30,000 h)	351.24	765.29	1613.3	270.42	599.87	1231.9	73.45	48.43	24.80

$Fe_{water1} = 5.2 \times 10^{-3}$ mmol/L, $Fe_{water2} = 10 \times 10^{-3}$ mmol/L, $Fe_{water3} = 20 \times 10^{-3}$ mmol/L

So the numerical model proposed here allows to describe the spatial distribution of iron incrustation using a simplified hypothesis for a given set of hydrodynamic and geochemical parameters.

The heterogeneous spatial distribution of well incrustations has been demonstrated by numerous qualitative observations taken from camera inspections and excavated wells (Houben and Treskatis 2007). The general pattern described for ochre deposits showing a growing mass from the upper part of the screen is likely to be the one described by the numerical model proposed here. From numerical models developed for other processes, Houben (2006) has obtained similar results for the patterns of scales. According to his approach, the hydraulic background of the incrustation processes that can occur in a pumping well in natural groundwater flow are described in particular. He demonstrates that the main part of the deposit occurs also in the upper part of the screen and in the part of the well facing the natural direction of groundwater flow. Different processes lead to qualitatively similar results as pointed here. Moreover, this seems emphasize the fact that the distributions of iron incrustation computed by each approach and for each phenomenon are consistent with the patterns observed from scarce field investigations (Houben and Weihe 2009). This highlights an opportunity to build more realistic models with a higher level of complexity to include these various processes.

To proceed to a quantitative estimation of productivity loss caused by iron precipitation due to over-exploitation of a well and corresponding de-watering, the spatial distribution of scaled mass is not sufficient. Pore clogging and associated reduction in hydraulic conductivity must be estimated. Several models exist to link pore filling by a new mineral phase to evolution of permeability (Saripalli et al. 2001; Emmanuel and Berkowitz 2005; Houben and Treskatis 2007). All three analyses are based on the Kozeny-Carman equation (Bear 1979):

$$K = \frac{1}{5M^2}\left(\frac{\rho_w g}{\mu}\right)\left(\frac{n^3}{(1-n)^2}\right) \tag{10}$$

where n is the porosity of the porous medium, M is the specific surface of the iron particles (ratio of surface area to

bulk volume), ρ_w is the density of water, g is the gravitational constant, and μ is the absolute viscosity of water.

Changes in the specific surface between the initial and final steps are due to iron precipitation, which take place during mineral fouling induced by the de-watering process. This relationship is a complex function of the geometry of iron particles, the shape of secondary minerals and the location of mineral precipitates. These changes are difficult to quantify. So, conservative approach is retained in which M is considered constant during the fouling process. Considering the initial homogeneous hydraulic conductivity K_0 and the initial porosity n_0 for the aquifer medium, the new conductivity K_t at time t can be expressed as a function of the new porosity n_t (Li et al. 2005, 2006):

$$K_t = K_0 \frac{\left[\frac{n_0 - \Delta n_t}{n_0}\right]}{\left[\frac{1 - n_0 + \Delta n_t}{1 - n_0}\right]} \tag{11}$$

In this expression, only mineral precipitation is assumed to contribute to the change in porosity, as stated in the initial hypothesis of our model. The reduction of hydraulic conductivity is non-linearly related to the reduction in porosity (i.e. the rate of decrease in hydraulic conductivity increases as the porosity reduction becomes larger).

The bulk density of the ferrous oxide well incrustation is chosen as 1.25 g/cm^3. This value is different from the mineral densities of goethite or ferrihydrite (4.26 g/cm^3 and 3.96 g/cm^3, respectively), but volume corrections are needed due to the high water content of natural precipitates (Houben 2004). Equation 11 is then used to obtain the spatial distribution of hydraulic conductivity under de-watering conditions corresponding to 10 years of exploitation. Chemical conditions correspond to the worst case of chemical fouling, i.e. for interstitial water with higher iron contents. The initial spatial distribution of hydraulic conductivity and porosity is homogeneous ($K_0 = 5 \times 10^{-5}$ m s^{-1} and $n_0 = 0.25$, respectively).

Naturally, the final field of hydraulic conductivity gives the same pattern as for ferrous oxide deposits (Fig. 10). The minimum conductivity is found on the well axis, 1.5 m below the aquitard bottom and at the point of contact between the aquitard bottom and aquifer top which lies

Fig. 10 Vertical 2D distribution of hydraulic conductivity field in log scale after the equivalent of 10 years of de-watering conditions for interstitial water 3 (ferrous iron $= 20 \times 10^{-3}$ mmol/L)
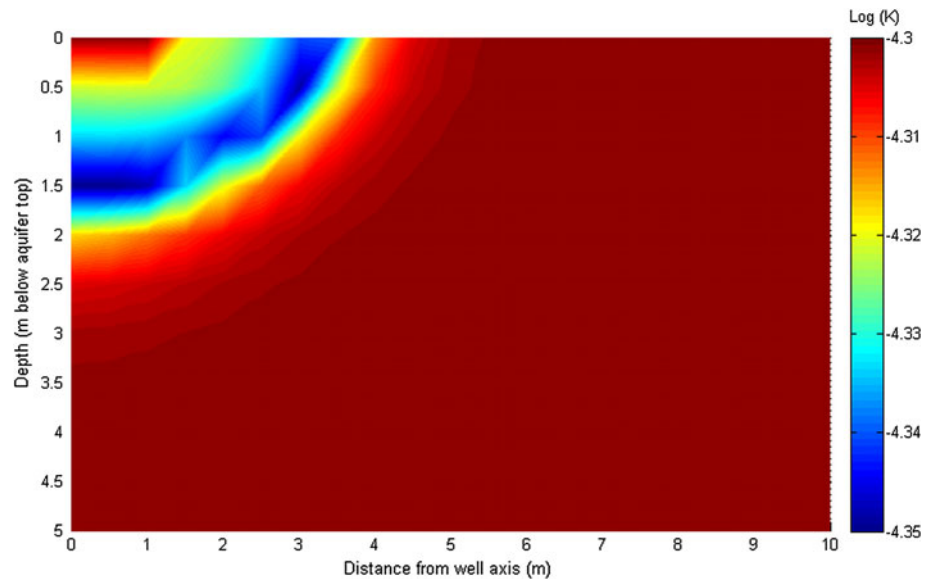
between 2.50 and 3.50 m from the well axis. The minimum value obtained is 4.37×10^{-5} m s^{-1}. The area of influence remains very localized as the magnitude of permeability varies. From the final conductivity field, it is possible to estimate the productivity of the well from the numerical model and to compare this with the initial productivity. For a fixed production rate, the difference in drawdown between the initial and final conditions gives the productivity loss induced by chemical clogging. For the worst case (interstitial water 3), this loss of productivity is of the order of 2% for 10 years of exploitation.

The calculated value of productivity loss is low. From this initial result, we can suppose that the influence of chemical clogging induced by the de-watering process is of minor importance for well ageing. The total mass of iron oxide deposited during the processes is limited and does not have much final impact on porosity. Moreover, the region affected by the clogging effect is not much developed, so the impact on the complete transmissivity of the aquifer remains small. This point must be discussed further because the spatial distribution of iron deposits seems to be of major importance to the evolution of productivity. For iron deposits localized very close to the well screen, clogging can be more harmful because of the higher velocity of groundwater flow.

In the coupled model developed here, the spreading of the clogging area is partly controlled by dispersivity. Several simulations were carried out for various sets of dispersivity data, keeping the same ratio of 1/10 between lateral and vertical dispersivity. The model remains sensitive to this parameter as highlighted by some of the results from these simulations (Fig. 11). The reference set of transport parameters corresponds to the base case used in the model with a mean value of 2 m for horizontal
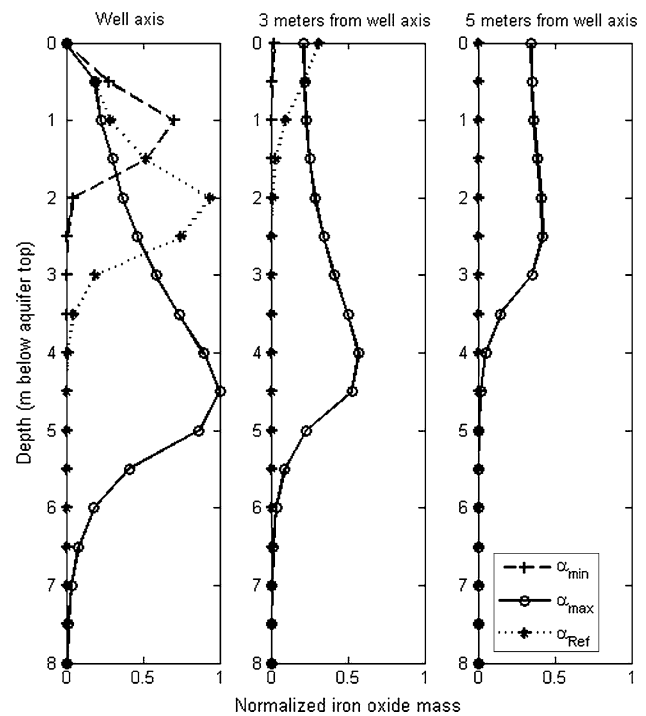

Fig. 11 Normalized iron mass precipitated for different values of horizontal dispersivity ($\alpha_{min} = 1$ m, $\alpha_{max} = 4$ m, $\alpha_{ref} = 2$ m) at different distances from well axis

dispersivity. Two simulations with different multiplication factors ($\times 2$ and $\times 0.5$, respectively) are presented. For each model, precipitated values of iron oxide are normalized to the maximum value of the domain. This value is generally found on the well axis. Results are given on the well axis and off-axis at distances of 3 and 5 m from the well axis. Of course, the spreading of the area of deposits is directly related to dispersivity, as demonstrated by the maximum

volume reached for the higher values of dispersivity ($\alpha_l = 4$ m and $\alpha_v = 0.4$ m). However, the local concentration of iron deposits is inversely proportional to dispersivity. The simulations done with models that integrated the lower dispersivity led to the highest masses of iron oxide. These observations emphasize the fact that the spatial pattern of oxide deposits induced by de-watering is strongly connected to the values of transport parameters. Usually, the lack of knowledge and data for this quantity lead to difficulties in integrating them into a numerical model.

The sensitivity study calls highlights two points. Firstly, for low dispersivity media, iron oxide is precipitated in the immediate vicinity of the de-watered area, at the highest concentration. This can lead to pore volumes that are efficiently filled on a local scale, especially at the top of the screen. The damaged area as a percentage of the whole screen should be low, especially for thick aquifers. This case should lead to limited impact on productivity for long exploitation schemes. Secondly, for more dispersive porous media, the volume filled by iron oxide is greater at lower concentrations. The part of the screen damaged by the oxide deposits is more extensive. The impact on well productivity, however, as highlighted by the models, remains of minor importance.

However, the model is not able to represent the complex hydraulic behaviour in the region closest to the well, at the interface between well and aquifer or screen and gravel pack, where slight modifications of conductivity can lead to dramatic effects on well productivity (Houben and Treskatis 2007).

Conclusions

For a great deal of water supply, the maintenance of water wells has become more important than the creation of new ones and so water well ageing is now an essential question. Interacting with the heterogeneous natural environment, the water well remains a complex system which can be affected by several processes leading to a general decrease in production yield. Among these, chemical clogging is of prime importance. Thus, de-watering conditions for confined aquifers induced by inappropriate exploitation schemes can induce the precipitation of new mineral phases leading to a general decrease in well productivity.

A numerical model representative of a theoretical well exploiting a confined aquifer was built to assess the potential impact of de-watering on the evolution of productivity. Geochemical and transport processes were taken into account. The approach presented here is based on simple hypotheses but developed from real-life systems.

The case of the precipitation of carbonates and iron oxide, one of the most common causes of chemical incrustation (Saripalli et al. 2001), was studied for a varied set of interstitial waters. The results emphasize two major points. First, the contribution to carbonate scales made by de-watering processes is of minor importance. It must be pointed out that this observation is conditioned by the choice of the modelling framework. It appears that the precipitation of carbonate is mainly induced by the increasing flow velocities in close proximity to the well leading to a release of CO_2. The model cannot simulate this effect. However, this process is not connected directly to the de-watering issue.

Secondly, the complex distribution of iron oxide deposits is emphasized. A major part is formed on the well axis, in the upper part of the screen. This local pattern seems to be in accordance with some observations made during video inspection of damaged exploitation wells (Stuetz and McLaughlan 2004). Iron deposits also occur at a distance from the well axis; at the contact point of aquifer and aquitard bottom, the contents of water get dissolved as iron. The general pattern is due to the difference between the rate of precipitation, linked to iron concentration, and the diffusion of oxygen in the aquifer from the de-watered area. The lower the concentration, the farther and deeper the precipitation occurs.

The quantities of iron oxide incrustation computed are used to estimate pore filling and the evolution of hydraulic conductivity by means of a simplified permeability model. A long-term simulation corresponding to 10 years of exploitation under de-watering conditions is carried out. In the worst case, the new distribution of hydraulic conductivity leads to a weak variation of productivity of the order of 2%.

The results obtained are strongly affected by the transport parameters used in the simulation as highlighted by the sensitivity analysis. The lack of data on this scale for exploitation wells/aquifer configuration is a major limitation for further investigations. Moreover, some limitations appear due to the assumptions made in the model, mainly in the geochemical/transport part of the model, as some of the processes were necessarily simplified. The major limitation concerns the hydraulic behaviour of iron oxide following precipitation. No transport of the colloidal iron particles is considered. The movement of the new mineral phases towards the well should lead to greater filling of the porous media in the gravel pack or directly against the screen. This characterization would require a more accurate description of the physical behaviour of particle transport, which is not possible on the scale used for this study as it demands a very detailed description of the contact between well and aquifer. This development should allow an accurate description of degassing phenomena for

dissolved gases such as carbon dioxide. Thus, the prediction of carbonate precipitation should be improved in equal measure.

The part played by biological agents in the geochemical processes should also be addressed, especially with regard to the auto-catalytic character of some of the material deposition processes (Houben and Treskatis 2007) which has not been considered in the geochemical model given here. This feature is expected to increase the quantity of deposited material leading to a higher decrease in productivity for long-term exploitation. Moreover, the real part played by biological slime in the clogging of porous media should be taken into account. Recent works investigate the importance of this phenomenon (Brovelli et al. 2009; Thullner et al. 2004) by relating the filling of pore space due to the microbial biomass forming continuous biofilms or isolated colonies. Thus, a direct link between microbial growth and reduction of permeability can be incorporated by including specific parameters for the micro organism description such as biomass growing factor, biomass decay rate, etc. (Soleimani et al. 2009). The connection of this kind of model to physico-chemical approaches should increase our general understanding of well ageing under different exploitation conditions.

Nevertheless, despite these limitations, the model described here does point out the potential minor part played by the de-watering process in the loss of productivity of some over-exploited wells in confined aquifers. De-watering of confined wells must be controlled for other practical reasons (physical damage to well structure), but the fact remains that chemical clogging due to local de-watering of the well has only a limited impact on the classical exploitation scheme.

From a general point of view, this approach represents a step forward towards a quantitative assessment of the aquifer/well system behaviour for the practical purposes of ageing assessment. A combination of models describing physical and chemical processes, and most probably other models including biological effects should lead to an assessment of the future damage done by pumping wells and should suggest ways for better managing these systems. Accordingly, a lot of additional research and quantitative monitoring is necessary so as to build a complete modelling approach, representative of the complex reality out in the field.

References

Andre L (2002) Contribution de la géochimie à la connaissance des écoulements souterrains profonds—application à l'aquifère des Sables Infra-Molassiques, PhD thesis, Bordeaux 3

Barrash W, Clemo T, Fox JJ, Johnson TC (2006) Field, laboratory, and modeling investigation of the skin effect at wells with slotted casing, Boise Hydrogeophysical Research Site. J Hydrol 326:181–198

Bear J (1979) Hydraulics of Groundwater. Mcgraw-Hill, New York

Boggs JM, Young SC, Beard LM, Gelhar LW, Rehfeldt KR, Adams EE (1992) Field study of dispersion in a heterogeneous aquifer, 1, overview and site description. Water Resour Res 28:3281–3291

Brovelli A, Malaguerra F, Barry D (2009) Bioclogging in porous media: model development and sensitivity to initial conditions. Environ Model Softw 24:611–626

Douez O (2007) Réponse d'un système aquifère multicouche aux variations paléclimatiques et aux sollicitations anthropiques—approche par modélisation couplée hydrodynamique, thermique et géochimique, PhD thesis, Bordeaux 3

Driscoll FG (1986) Groundwater and wells. Reynolds Guyar, New York

Durlofsky LJ (2000) An approximate model for well productivity in heterogeneous porous media. Math Geol 32:421–438

Emmanuel S, Berkowitz B (2005) Mixing-induced precipitation and porosity evolution in porous media. Adv Water Resour 28:337–344

Freedman VL, Saripalli KP, Bacon DH, Meyer PD (2005) Implementation of biofilm permeability models for mineral reactions in saturated porous media. Comput Geosci 31:968–977

Gelhar LW, Welty C, Rehfeldt KR (1992) A critical review of data on field-scale dispersion in aquifers. Water Resour Res 28:1955–1974

Han G, Dusseault MB (2003) Description of fluid flow around a wellbore with stress-dependent porosity and permeability. J Petrol Sci Eng 40:1–16

Hitchon B (2000) "Rust" contamination of formation waters from producing wells. Appl Geochem 15:1527–1533

Houben GJ (2003a) Iron oxide incrustations in wells. Part 1. Genesis, mineralogy and geochemistry. Appl Geochem 18:927–939

Houben GJ (2003b) Iron oxide incrustations in wells. Part 2. Chemical dissolution and modeling. Appl Geochem 18:941–954

Houben GJ (2004) Modeling the buildup of iron oxide encrustations in wells. Ground Water 42:78–82

Houben GJ (2006) The influence of well hydraulics on the spatial distribution of well incrustations. Ground Water 44:668–675

Houben G, Treskatis C (2007) Water well—rehabilitation and reconstruction. McGraw-Hill, New York

Houben GJ, Weihe U (2009) Spatial distribution of incrustations around a water well after 38 years of use. Ground Water. doi: 10.1111/j.1745-6584.2009.00641.x

Hsieh PA, Winston RB (2002) User's guide to model viewer, a program for three-dimensional visualization of ground-water model results. US Geological Survey Open-File Report 02-106

Kipp KL (1987) HST3D: a computer code for simulation of heat and solute transport in three-dimensional ground-water flow systems. US Geological Survey Water-Resources Investigations Report 86-4095

Larroque F (2004) Gestion globale d'un système aquifère complexe—application à l'ensemble multicouche nord-médocain, PhD thesis, Bordeaux 3

Larroque F, Treichel W, Dupuy A (2008) Use of unit response functions for management of regional multilayered aquifers: application to the north aquitaine tertiary system (France). Hydrogeol J 16:215–233

Leung CM, Jiao J, Malpas J, Chan W, Wang Y (2005) Factors affecting the groundwater chemistry in a highly urbanized coastal area in Hong Kong: an example from the mid-levels area. Environ Geol 48:480–495

Li L, Benson CH, Lawson EM (2005) Impact of mineral fouling on hydraulic behaviour of permeable reactive barriers. Ground Water 43:582–596

Li L, Benson CH, Lawson EM (2006) Modeling porosity reductions caused by mineral fouling in continuous-wall permeable reactive barriers. J Contam Hydrol 83:89–121

Millero FJ (1985) The effect of ionic interactions on the oxidation of metals in natural waters. Geochim Cosmochim Acta 49:547–553

Millero FJ, Sotolongo S, Izaguirre M (1987) The oxidation kinetics of Fe(II) in seawater. Geochim Cosmochim Acta 51:793–801

Parkhurst D, Appelo CA (1999) User's guide to PHREEQC (Version 2): a computer program for speciation, reaction path, 1D-transport and inverse geochemical calculations. US Geological Survey Water Investigation Report, pp 99–4259

Parkhurst DL, Kipp KL, Engesgaard P, Charlton SR (2004) PHAST—a program for simulating ground-water flow, solute transport, and multicomponent geochemical reactions. US Geological Survey Techniques and Methods 6-A8

Plummer LN, Wigley TM, Parkhurst DL (1978) The kinetics of calcite dissolution in CO2-water systems at 5° to 60°C and 0.0 to 1.0 atm CO2. Am J Sci 278:179–219

Powers JP, Corwin AB, Schmall PC, Kaeck WE (2007) Long-term dewatering systems construction dewatering and groundwater control, 3rd edn. Wiley, USA, pp 572–576

Saripalli KP, Meyer PD, Bacon DH (2001) Changes in hydrologic properties of aquifer media due to chemical reactions: a review. Crit Rev Environ Sci Technol 31:311–349

Singer LN, Stumm W (1970) The solubility of ferrous iron in carbonate-bearing waters. J Am Water Works Assoc 62:202–298

Soleimani S, Geel PJ, Isgor OB, Mostafa MB (2009) Modeling of biological clogging in unsaturated porous media. J Contam Hydrol 106:39–50

Stuetz RM, McLaughlan RG (2004) Impact of localised dissolved iron concentrations on the biofouling of environementals wells. Water Sci Technol 49:107–113

Sun NZ (1996) Mathematical modeling of groundwater pollution. Springer, New York

Sung W, Morgan JL (1980) Kinetics and product of ferrous iron oxygenation in aqueous systems. Environ Sci Technol 14:561–568

Tamura H, Goto G, Nagayama M (1976) The effect of ferric hydroxide on the oxygenation of ferrous ions in neutral solutions. Corros Sci 16:197–207

Thullner M, Schroth MH, Zeyer J, Kinzelbach W (2004) Modeling of a microbial growth experiment with bioclogging in a two-dimensional saturated porous media flow field. J Contam Hydrol 70:37–62

Walter DA (1997) Geochemistry and microbiology of Iron-related well-screen encrustation and aquifer biofouling in Suffolk County, US Geological Survey Water Resource Investigate Report, Long-island, 97-4032

Winston RB (2006) GoPhast: a graphical user interface for PHAST. US Geological Survey Techniques and Methods 6-A20

Wu J, Wu Y, Lu J (2008) Laboratory study of the clogging process and factors affecting clogging in a tailings dam. Environ Geol 54:1067–1074